Available online at www.sciencedirect.com

ScienceDirect

Geochimica et Cosmochimica Acta 150 (2015) 253–264

Geochimica et Cosmochimica Acta

www.elsevier.com/locate/gca

Sulfur-controlled iron isotope fractionation experiments of core formation in planetary bodies

A. Shahar [a,*], V.J. Hillgren [a], M.F. Horan [b], J. Mesa-Garcia [a,c], L.A. Kaufman [a], T.D. Mock [b]

[a] Geophysical Laboratory, Carnegie Institution of Washington, Washington, DC 20015, USA
[b] Department of Terrestrial Magnetism, Carnegie Institution of Washington, Washington, DC 20015, USA
[c] Geology Department, Universidad EAFIT, Medellin, Colombia

Received 5 May 2014; accepted in revised form 12 August 2014; available online 23 August 2014

Abstract

A series of high pressure and temperature experiments were conducted to better constrain the Fe isotope fractionation during core–mantle differentiation in planetesimal and planetary bodies. Synthetic mixtures of oxides and metal having varying amounts of sulfur, approximating terrestrial and Martian compositions, were melted at 1–2 GPa and 1650 °C. Iron isotopic equilibrium between the resulting metal and glass run products was verified for all experiments using the three-isotope technique. Purified Fe from metal and glass was analyzed by multiple-collector ICP-MS in high resolution mode. Iron alloy and silicate glass show a well-resolved $\Delta^{57}Fe_{metal-silicate}$ of $+0.12 \pm 0.04‰$ in a sulfur-free system. Isotope fractionation increases with sulfur content to $+0.43 \pm 0.03‰$ at 18 wt.% sulfur in the metal. These results cannot be easily interpreted within the context of known Fe isotope ratios in most natural samples of planetary and asteroidal mantles and therefore suggest more complex processes affected the Fe isotope fractionation therein. However, to reconcile Martian meteorite iron isotopic signatures with geophysical models using this new experimental data requires a smaller amount of sulfur in the Martian core than previous estimates, with an upper limit of ~8 wt.%.

1. INTRODUCTION

Differentiation of a silicate mantle and metallic core occurred on the terrestrial planets, the moon and on many asteroids, as these objects were hot and big enough to melt the metal so it could percolate through the silicate (Taylor, 1992). The necessary heat largely comes from energy released during radioactive decay. The iron and siderophile elements sink to the center to form a core, while the silicates and lithophile elements form a mantle. Many details of differentiation processes are still unclear, but may be constrained by numerical modeling (e.g., Lodders, 2000; Moskovitz and Gaidos, 2011; Elkins-Tanton, 2012), laboratory experimental work (e.g., Rushmer et al., 2005; Chabot et al., 2011) and analysis of natural samples (e.g., Kleine et al., 2005; Caro et al., 2006; Borg et al., 2011).

The distinct chemical bonding environments of elements in different phases are expected to induce isotope fractionation of these elements. For example, Fe in planets and planetesimals should manifest isotope fractionation resulting from core–mantle differentiation. In theory, the fractionation should constrain the bulk chemical composition of the planetary body and the composition and conditions of differentiation of unseen reservoirs like the core. In practice, interpretation of Fe isotope compositions of natural samples is less than straightforward. Iron in terrestrial abyssal peridotites (Craddock et al., 2013) has a similar

* Corresponding author.
E-mail address: ashahar@ciw.edu (A. Shahar).

http://dx.doi.org/10.1016/j.gca.2014.08.011
0016-7037/

isotope composition to most chondrites (Dauphas et al., 2009; Craddock and Dauphas, 2010). Shergotty–Nahkla–Chasigny (SNC) meteorites from Mars and eucrite–diogenite (HED) meteorites thought to originate on the asteroid Vesta, also have chondritic iron isotope values (Poitrasson et al., 2004; Wang et al., 2012). By contrast, Fe in peridotite xenoliths (Poitrasson et al., 2013), and in terrestrial basalts (e.g., Teng et al., 2013; Craddock et al., 2013) is enriched in the heavier isotopes by ~0.1‰ in $^{57/54}$Fe. These contrasts lead to uncertainties regarding the Fe isotope composition of the bulk silicate Earth, the isotopic effect of partial mantle melting in planet and planetesimals, and the extent of isotope fractionation during core–mantle differentiation.

Theoretical calculations (Polyakov, 2009) and laboratory experiments do not yet provide a consistent answer of whether iron should be isotopically fractionated during core–mantle differentiation. There are three previous experimental studies that constrain mass fractionation of Fe between Fe metal and magnesian silicate at high temperatures and pressures. Poitrasson et al. (2009) and Hin et al. (2012) suggested that fractionation was not resolvable between metal and silicate in their experiments, and Williams et al. (2012) inferred a large fractionation from their experimental results, which were conducted at higher pressure and oxygen fugacity conditions. We undertook a carefully-designed set of experiments to re-evaluate iron mass fractionation between metal and silicate during melting. In order to better simulate differentiation under natural conditions, we focus on the isotopic effect of adding a light element, in this case sulfur, to the metal.

Terrestrial seismic data supports the presence of light elements in addition to Fe within the core of the Earth. The main candidates considered are carbon, sulfur, oxygen, silicon and hydrogen. The elements with which molten Fe metal bonds during core–mantle differentiation is a function of the conditions attending the core formation. For example, at high temperature under reducing conditions, Si is likely to alloy with iron (Ricolleau et al., 2011); under more oxidizing conditions, however, sulfur is likely to enter the metal (Sanloup and Fei, 2004). The presence of substantial sulfur has long been inferred for the Martian core (Wänke and Dreibus, 1988). Trace element contents of iron meteorites that require sulfur during crystallization imply its importance in many asteroidal cores (e.g., Chabot, 2004). For these reasons, we chose to evaluate the effect of sulfur on the mass fractionation of Fe during laboratory experiments similar to differentiation.

2. METHODS

2.1. Experimental setup

Experiments were conducted in a piston cylinder apparatus at the Geophysical Laboratory at 1 and 2 GPa. The ½" piston cylinder assembly consisted of a graphite tube heater insulated with a Pyrex glass sleeve surrounded by a talc shell. The samples were contained in BN capsules or MgO capsules. Due to interaction with the capsule, discussed below, only one experiment in an MgO capsule was found to have equilibrated and therefore that is the only experiment in an MgO capsule for which we provide the isotopic analyses. The temperature was measured with a W/Re thermocouple in contact with the top of the sample capsule. All runs were conducted at 1650 °C. Run durations were varied from 5 to 150 min. The quench times were measured and a temperature of 200 °C was obtained in less than 10 s after power was cut from the experiment.

Two different starting materials were used: Mars-like and Earth-like. The Earth experiments consisted of 69 wt.% of an oxide mix and 31 wt.% of pure Fe metal. These experiments were conducted in MgO capsules. However, as noted above, only one of these experiments came to isotopic equilibrium. The Mars-like experiments consisted of 78 wt.% of an oxide mix and 22 wt.% of a mixture of FeS, Fe, and Ni. The metal contained 17, 10, 5 or 0 wt.% S. The starting silicate compositions are given in Table 1. Duplicate experiments with 10 wt.% sulfur were done to double check equilibrium conditions and to evaluate whether a pressure difference of 1 and 2 GPa affects the iron isotopic fractionation.

2.2. Chemical analyses of the experimental charges

After each experiment, the capsule was broken in half. One side of the experiment was polished and analyzed for its chemical composition using instrumentation at the Carnegie Institution of Washington discussed below. The pieces of glass and metallic beads chosen for sample characterization were set in epoxy and polished for analysis (Fig. 1). Results are provided in Table 2.

Metal was analyzed using a JEOL 6500F Field Emission scanning electron microscope (SEM) outfitted with an Oxford X-Max 80 mm^2 Si Drift Detector combined with an Aztec software package. Use of the SEM provided high accuracy for the metal compositions, because the metal quenched to a dendritic pattern. Analyses were made over large representative areas of the quenched metal for 50 s, using an accelerating voltage of 15KeV and a beam current of 1 nA. Standards were pure Fe metal, pure Ni metal, pyrite, and BN. The Si-drift detector provides higher sensitivity and lower detection limits (to 0.05% for Fe (John Armstrong, personal communication)) compared to standard EDS. Oxygen detected in the metal samples resulted from oxidation of the metal surface during preparation for analysis.

Table 1
Starting compositions of the silicate fractions.

Composition 1 "Earth-like"	Oxide (wt.%)	Composition 2 "Mars-like"	Oxide (wt.%)
SiO_2	47.9	SiO_2	46.5
MgO	36.2	MgO	29
Fe_2O_3	6.4	FeO	17.6
Al_2O_3	3.8	Al_2O_3	2.8
CaO	5.6	CaO	2.4
^{54}FeO	~0.1	^{54}FeO	~0.1
		Na_2O	1.0

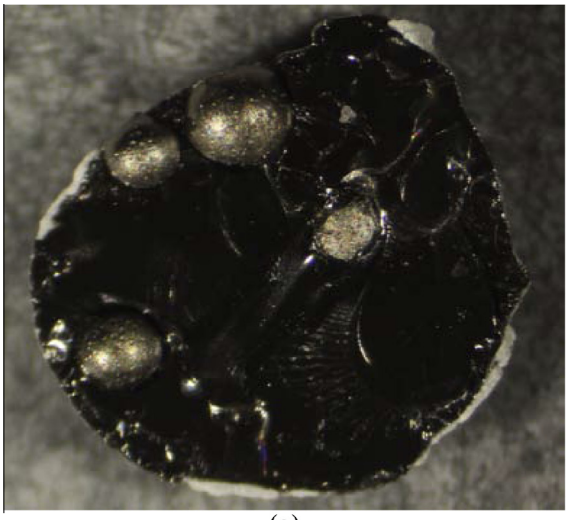

(a)

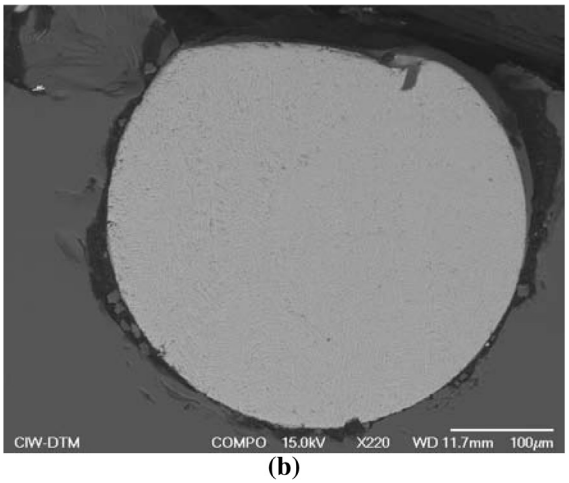

(b)

Fig. 1. (a) Image of a sample broken in half after the experiment, showing the Fe–S alloy and the silicate glass. The diameter of the capsule is approximately 3 mm. (b) Backscatter Electron Image of a polished portion of run PC1008 showing the quenched silicate glass and Fe–S metallic alloy. The alloy consists of 2–4 μm intergrowths of Fe-metal and a sulfide that form upon quench. The silicate is a glass and devoid of quench features.

Glass and silicates were analyzed with a JEOL 8900 electron microprobe, using an accelerating voltage of 15KeV and beam current of 30 nA. The beam was rastered over an area of approximately 15 microns square. Counting times ranged from 30 to 90 s. Standards were a forsteritic olivine (Fe in the glass, Mg, Si, and O), Sillimanite (Al), Wollastonite (Ca), Kaerstutite (Na), Pyrite (S), BN (N), NIST K326 (B), pure Fe (Fe in the metal) and pure Ni (Ni in the metal). Nickel contents in the glasses were below the detection limit of 80 ppm.

Boron contents in the silicate glass for runs PC1008, PC1011, PC1012, and PC1036 were measured by Cameca IMS 6F small-radius secondary ion microprobe (SIMS), using a 10 nA primary ion beam of oxygen. Primary beam width was 10–15 μm, and secondary ions were detected with a nominal acceleration voltage of +10 kV. Energy filtering was employed (-165 ± 50 eV) and the calibration performed using NIST SRM, NIST K326 and MPI-DING glasses (Leroux et al., 2006). Detection limit for boron was 0.2 ppm, measured using Suprasil 3001 glass. Combined accuracy and precision is ±7% (2σ). These boron contents then were used to recalculate the glass compositions measured using the microprobe.

2.3. Iron isotope analyses of the experimental charges

Silicate glass and metal fractions were handpicked from the unpolished portion of each experimental charge. Iron metal and silicates have different visual properties, so that they could be easily mechanically separated. The S-bearing metallic alloy quenched to large metallic beads. These beads could not be ground or disaggregated, and were further processed intact. The silicate fractions were further purified using a strong magnet to ensure that they contained no large metal inclusions, which could compromise measurement of the Fe isotope compositions of the silicate. It is important to note, as shown in Fig. 1, that the experiments in BN capsules (i.e., all the sulfur bearing experiments) resulted in a silicate glass with no additional silicate phases, making the silicate glass even easier to separate from the metal.

Silicates were dissolved in HF–HNO_3, and refluxed twice in 9 M HCl. Metal separates were dissolved in HCl–HNO_3, and refluxed twice in 9 M HCl. Iron was purified using 0.3 mL of anion exchange resin (BioRad AG-1×8, 100–200 mesh) in 9 M HCl and collected in 0.5 M HCl. The purified Fe was dried, and then redissolved in 0.5 M HNO_3 prior to analysis. This is a similar procedure to that in, e.g., Strelow (1980). A synthetic solution similar to the composition of the run products showed no isotopic fractionation of Fe when processed using this separation procedure.

Isotopic analyses were conducted on the Nu Plasma II at the Geophysical Laboratory. The instrument has a fixed array of 16 Faraday collectors each with amplifier resistors of 10^{11} Ω. Corrections for instrumental mass bias were obtained by using sample-standard bracketing with peak height matching between sample and standard to better than 5%. Samples and standards were analyzed as ~4 ppm Fe in 2% HNO_3 solutions aspirated through a DSN-100 desolvating nebulizer (Nu Instruments). Mass interferences from ArO^+, $ArOH^+$, and ArN^+ were resolved from $^{56}Fe^+$, $^{57}Fe^+$ and $^{54}Fe^+$, respectively, by operating at a high mass resolving power. Long-term reproducibility of our internal standard was <0.01‰/a.m.u when compared to IRMM-14. The sample solutions first were checked for $^{52}Cr^+$ and in each case the intensity was found to be less than 2 mV, indicating that $^{54}Cr^+$ interference on $^{54}Fe^+$ was negligible. Additional instrumental mass bias due to inter-element matrix effects was not an issue for these purified solutions. Typical precision for a single analysis of a Fe solution (~4 ppm in 2% HNO_3) is ±0.04‰/a.m.u (2std). Samples were analyzed 6 to 10 times with each analysis consisting of 20 cycles of ~4 s integrations. Metal and silicate samples from the same experiment were measured on the same day, and then re-analyzed on a different day to verify reproducibility over time.

Table 2
The composition of the run products and Fe isotope compositional data for all experiments from this study plotted in Fig. 3.

	PC1008	PC1011	PC1012	PC1036	PC1195	PC978	
Pressure	1 GPa	1 GPa	1 GPa	2 GPa	1 GPa	1 GPa	
Temperature	1650 °C	1650 °C	1650 °C	1650 °C	1650 °C	1650 °C	
Run duration	120 min	120 min	120 min	150 min	120 min	120 min	
Silicate	Glass[a]	Glass[a]	Glass[a]	Glass[a]	Glass[a]	Liquid[a]	Olivine[a]
Si	21.85 ± 0.08	21.39 ± 0.06	21.11 ± 0.05	19.59 ± 0.16	22.51 ± 0.14	17.23 ± 0.08	19.31 ± 0.09
Mg	15.17 ± 0.09	16.44 ± 0.12	17.44 ± 0.11	20.33 ± 0.31	13.70 ± 0.10	18.90 ± 0.58	31.99 ± 0.24
Fe	6.61 ± 0.17	7.04 ± 0.05	6.10 ± 0.14	3.56 ± 0.42	6.88 ± 0.25	8.21 ± 0.14	3.66 ± 0.14
Ca	2.12 ± 0.02	2.19 ± 0.02	2.18 ± 0.02	1.69 ± 0.03	1.81 ± 0.02	7.37 ± 0.33	0.30 ± 0.06
Al	1.22 ± 0.02	1.27 ± 0.02	1.32 ± 0.02	0.99 ± 0.02	1.15 ± 0.02	5.86 ± 0.24	0.13 ± 0.08
Na	0.33 ± 0.01	0.27 ± 0.01	0.30 ± 0.00	0.52 ± 0.01	0.74 ± 0.01	NP	NP
O	45.79 ± 0.18	45.90 ± 0.16	45.21 ± 0.33	45.40 ± 0.43	46.91 ± 0.21	42.62 ± 0.12	44.38 ± 0.18
S	0.14 ± 0.01	0.07 ± 0.01	0.09 ± 0.01	0.16 ± 0.03	NP	NP	NP
N	1.31 ± 0.02	1.33 ± 0.12	1.37 ± 0.10	0.82 ± 0.19	0.95 ± 0.11	NP	NP
B[c]	4.09 ± 0.29	4.19 ± 0.29	4.14 ± 0.29	5.37 ± 0.04	4.55 ± 0.11	NP	NP
Total	98.63	100.08	99.26	98.44	99.21	100.19	99.77
Metal	Sulfide liquid[b]	Sulfide liquid[b]	Sulfide liquid[b]	Sulfide liquid[a]	Liquid metal[a]	Liquid Fe[a]	
Fe	78.21 ± 0.30	86.39 ± 0.28	79.61 ± 0.30	84.76 ± 0.12	93.03 ± 0.33	101.10 ± 0.48	
Ni	1.27 ± 0.18	2.71 ± 0.18	6.20 ± 0.22	4.10 ± 0.06	2.18 ± 0.04	NP	
S	17.51 ± 0.16	5.33 ± 0.08	9.80 ± 0.10	10.23 ± 0.11	NP	NP	
O	1.12 ± 0.12	1.66 ± 0.10	0.94 ± 0.10	0.35 ± 0.05	0.20 ± 0.02	0.32 ± 0.03	
N	1.89 ± 0.24	3.38 ± 0.20	3.30 ± 0.20	1.56 ± 0.19	2.92 ± 0.16	NP	
Total	100.00	99.48	99.84	101.00	98.62	101.42	
Log X_{FeO}/X_{Fe}	−1.03	−1.06	−1.09	−1.37	0	−1.09	
$\Delta^{57}Fe_{met-sil}$	0.43 ± 0.05	0.18 ± 0.03	0.33 ± 0.05	0.30 ± 0.04	0.137 ± 0.042	0.117 ± 0.038	

NP = not present.
[a] Microprobe analysis error is one standard deviation among multiple analyses.
[b] SEM analysis, error is two standard deviations of the total counts.
[c] Boron concentrations for runs PC1008, PC1011, PC1012, and PC1036 were determined by SIMS and errors are as described in the text. The B concentration for run PC1195 was determined by microprobe.

3. RESULTS

3.1. Description of the run products

For each experiment, Table 2 provides run conditions and chemical analyses of the resultant run products, as well as the Fe isotope fractionation between the metal and silicate phases. All the experiments conducted in BN capsules melted completely and quenched to a homogenous silicate glass with no quench features and multiple metal beads (see Fig. 1). In S-bearing runs the metallic beads have a quench texture that consist of 2–4 μm scale intergrown metal and sulfide dendrites. Both the metal and glass are contaminated with B and N from the capsules. In runs in MgO capsules, the silicate melt quenched to a dendritic texture and olivine was stabilized as a result of interaction of the charge with Mg from the capsule.

All experiments discussed here were closed systems with respect to iron. Our earlier experiments using MgO capsules typically resulted in loss of Fe to the capsule during the run. Fig. 2 compares an Fe map of the sample capsule interface of one of those experiments with an Fe map of an experiment that used a BN capsule. Because no iron was lost to BN capsules, all the experiments discussed here, except one, used BN capsules. Results of one experiment (PC978) in an MgO capsule for which we verified closed system behavior are provided for comparison.

We should also note, we were unable to break, grind or otherwise disaggregate the metallic beads. The beads remained intact during mechanical separation of the alloy and silicate, and until dissolution in acids prior to Fe purification. This implies that the quench features in the S-bearing metallic alloys (a troilite-like phase and an iron rich phase) cannot be separated from one another during grinding and therefore contamination of the silicate from either dendritic phase cannot be the reason for the fractionation found in this study.

Submicrometer-sized iron sulfides were found within the silicate glass, and comprise 0.3–0.4% of the total Fe in the glasses. These sulfides have been seen in previous experiments and are interpreted as being in equilibrium with the silicate during the conditions of the experiment and exsolving during quench. Wheeler et al. (2006) tested this interpretation by doping their experiments with palladium (which alloys readily with iron metal) and found that the tiny metallic blebs within the silicate had no resolvable palladium at the end of the experiment. Therefore, these 'blebs' were interpreted as dissolved in

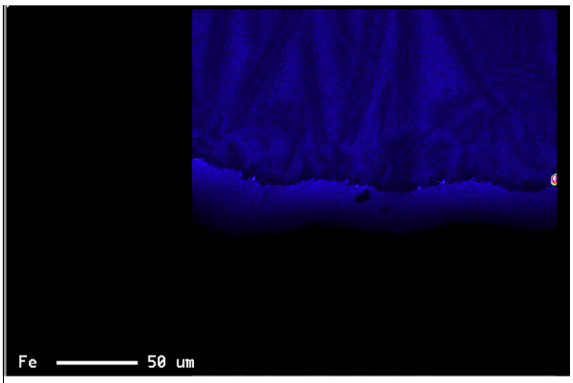

(a)

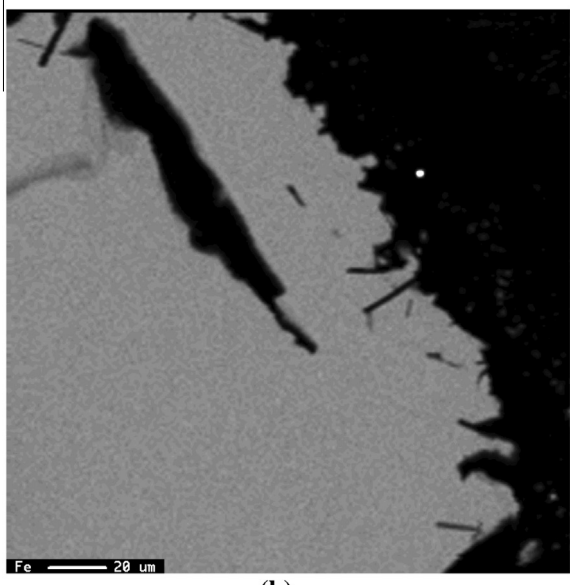

(b)

Fig. 2. Two images of sample–capsule contacts contrast loss of Fe to the MgO capsule versus the closed system in a BN capsule. (a) A BSE image with an Fe map overlain on the recovered sample and MgO capsule. The wavy area shows the contact between dendritic silicate liquid (top) and the MgO capsule (bottom). The MgO capsule shows iron incorporated into it forming (Mg, Fe)O. (b) A grayscale Fe map of a recovered sample in a BN capsule. The contact between the glass (left side, gray) and BN capsule (right side, black) is sharp with no Fe incorporated into the capsule.

the silicate portion during run conditions. It is important to consider the possibility that the iron sulfide blebs in the silicate glass in our experiments are not a quench product but an equilibrium metal phase. If the quench interpretation is incorrect and the blebs represent contamination of the silicate glass with the equilibrium metal phase, then their presence potentially could affect the Fe isotope compositions of the silicate glasses. In order for this isotopic effect to be resolvable (±0.02 per mil), the low abundance of these blebs (0.3–0.4%) in the silicate glasses, however, would require their Fe isotope composition to differ by >2 per mil from the glasses. Such an extent of mass fractionation has not been reported in similar experiments or in natural samples.

3.2. Oxygen fugacity

The fO_2 cannot be directly measured in these experiments. In metal–silicate systems, one normally calculates the fO_2 based on the oxidation/reduction reaction $Fe + ½ O_2 \Leftrightarrow FeO$ by comparing the activity of FeO in the silicate to the activity of Fe in the metal. When Fe is dissolved in a sulfur-bearing metallic liquid, however, the activity of Fe depends on its exact speciation in the liquid, which is unknown. In addition, contamination of the silicate liquid by B and N from the capsule prevents the use of well-calibrated oxygen fugacity monitors in silicates. As a proxy for more direct measurement of fO_2, we compare the distribution coefficient of Fe between metal and silicate in the run products. As shown in Fig. 4, the distribution coefficients vary little among the run products, suggesting that all had similar fO_2. However, if we were to calculate the fO_2 for these experiments using simply the mole fraction of Fe in the alloy, it yields an oxygen fugacity approximately 2 log units below the Iron-Wüstite buffer (IW-2) for all runs. We can also use a simple speciation model for the metal where we assume each S atom is associated with one Fe atom and each N atom is associated to three Fe atoms to calculate the activity of the Fe (see for example, Chabot and Jones, 2003). Using this activity for the Fe yields fO_2's between IW-1 and IW-2.

3.3. Fe isotope results

Iron isotope data are given in Table 3. Fig. 3 shows the iron isotope fractionation between metal and silicate ($\Delta^{57}Fe_{metal–silicate}$) as a function of the weight percent sulfur

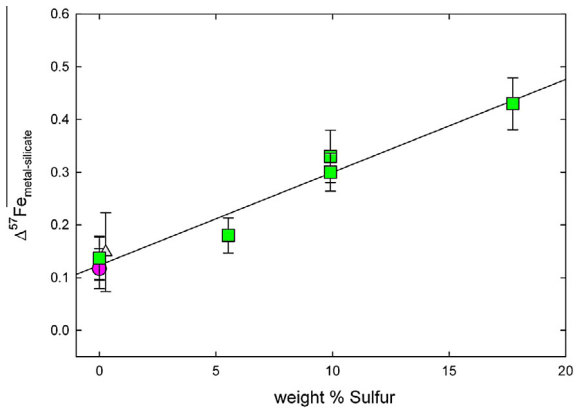

Fig. 3. $\Delta^{57}Fe_{metal–silicate}$ versus weight% sulfur in the experiment. $\Delta^{57}Fe_{metal–silicate}$ is the difference between the $\delta^{57}Fe$ of the metal and the $\delta^{57}Fe$ of the silicate. Starting compositions were Mars-like (green squares) and Earth-like (pink circle). The solid line is the regression through the green squares from this study. The gray triangle shows the result from experiment PC564 from the Poitrasson et al. (2009) study, corrected for temperature, which is consistent with our results. The Mars-like and Earth-like experiments with no sulfur provide identical Fe fractionation factors, suggesting that melt chemistry does not change the iron isotopic fractionation within error. (For interpretation of the references to color in this figure legend, the reader is referred to the web version of this article.)

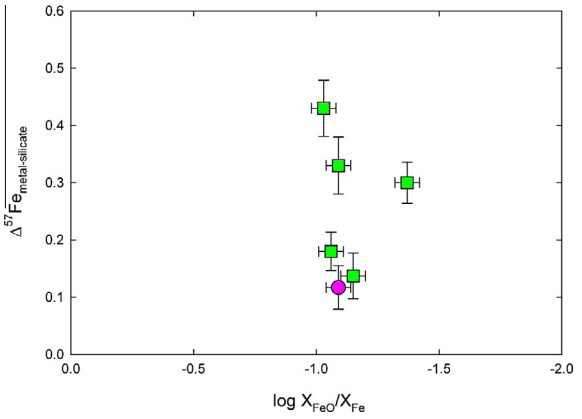

Fig. 4. $\Delta^{57}Fe_{metal-silicate}$ data plotted against calculated iron content in the silicate versus the metal in the experiments. The green squares represent the Mars-like experiments whereas the pink circle represents the Earth-like experiment. As there is no clear correlation in this figure between the oxidation state of the iron and the isotope fractionation it can be inferred that the inherent oxygen fugacity in the experiment is not causing the correlation with $\Delta^{57}Fe_{metal-silicate}$. (For interpretation of the references to color in this figure legend, the reader is referred to the web version of this article.)

in the metal alloy. Our experimental results show a resolvable Fe isotope fractionation between Fe alloy and silicate glass of $+0.12 \pm 0.04‰$ in a sulfur-free system. Isotope fractionation increases with sulfur content to $+0.43 \pm 0.03‰$ at 18 wt.% sulfur in the metal. Experiments with Mars-like and Earth-like starting compositions yield identical Fe isotope fractionations, suggesting that the chemical composition of the silicate does not affect the iron isotope fractionation within error.

In Figs. 4 and 5, we evaluate whether Fe isotopic fractionation may have been affected by variables in addition to S content. The Fe distribution coefficient, a proxy for fO_2, show no correlation with the magnitude of Fe isotope fractionation. The experiment at higher pressure (2 GPa) had the highest distribution coefficient, but yielded the same Fe isotope fractionation as those run at lower pressure (1 GPa). Similarly, Fig. 5a–d show that Fe isotope fractionation is independent of the amount of B or N contamination from the capsule in the silicate glass; the combined S and N contents of the metal; and the Ni content of the metal. A pair of experiments run at identical conditions but using a BN capsule and a MgO capsule also yielded Fe isotope fractionation factors well within error of each other (Table 3), suggesting that the compositions of the capsule material, so long as equilibrium is attained, also do not affect the results.

3.4. Demonstrating equilibrium

Proving that isotopic equilibrium has been obtained in the experiments is of utmost importance. In this study, we used the three-isotope exchange method, which incorporates an ^{54}Fe isotopic 'spike' to evaluate whether equilibrium had been achieved. Without the isotopic spike, reversal experiments would have to be done to prove equilibrium, which would require twice as many experiments and be less exact. Originally designed for low temperature aqueous work in which equilibrium is especially difficult to attain (Matsuhisa et al., 1978), the three-isotope method was extended to the determination of Fe isotope fractionation between minerals at high temperature and pressure (Shahar et al., 2008). By use of a spike, the three-isotope exchange method replaces the terrestrial fractionation line (TFL), which has a zero intercept with a secondary fractionation line (SFL) that has a non-zero intercept. The SFL has the same slope as the TFL but is displaced from it in proportion to the amount of added spike.

At isotopic equilibrium, all phases containing the element of interest must lie on the SFL. As derived in Shahar et al. (2008), for a plot of $\delta^{56}Fe$ versus $\delta^{57}Fe$, the slopes of the TFL and SFL are both 0.67795. The intercept can be calculated using,

Table 3
Fe isotope composition results.

	S (wt.%)		$\delta^{56}Fe$ (‰)	$\delta^{57}Fe$ (‰)	$\Delta^{56}Fe$ (‰)	$\Delta^{57}Fe_{metal-silicate}$
PC1008	17.51	Silicate	−12.92(.05)	−12.52(.06)	−4.43(.03)	0.43 ± 0.05
		Metal	−12.60(.06)	−12.09(.07)	−4.41(.03)	
PC1011	5.33	Silicate	−8.39(.03)	−8.01(.05)	−2.96(.04)	0.18 ± 0.03
		Metal	−8.26(.03)	−7.83(.04)	−2.95(.05)	
PC1012	9.80	Silicate	−13.04(.07)	−12.76(.08)	−4.41(.05)	0.33 ± 0.05
		Metal	−12.80(.07)	−12.43(.04)	−4.37(.07)	
PC1036	10.23	Silicate	−11.38(.06)	−11.07(.07)	−3.87(.04)	0.30 ± 0.04
		Metal	−11.15(.04)	−10.76(.03)	−3.86(.04)	
PC1195	0	Silicate	−7.58(.07)	−7.22(.07)	−2.68(.06)	0.14 ± 0.04
		Metal	−7.41(.07)	−7.09(.05)	−2.65(.02)	
PC978	0	Silicate	−2.66(.04)	−2.25(.04)	−1.13(.05)	0.12 ± 0.04
		Metal	−2.52(.03)	−2.13(.07)	−1.08(.02)	

All data are given in per mil. Uncertainties are 2^* standard errors of 8–10 analyses. $\Delta^{57}Fe_{metal-silicate}$ is calculated by subtraction; the error on this value includes uncertainties on $\delta^{56}Fe$ and $\delta^{57}Fe$.

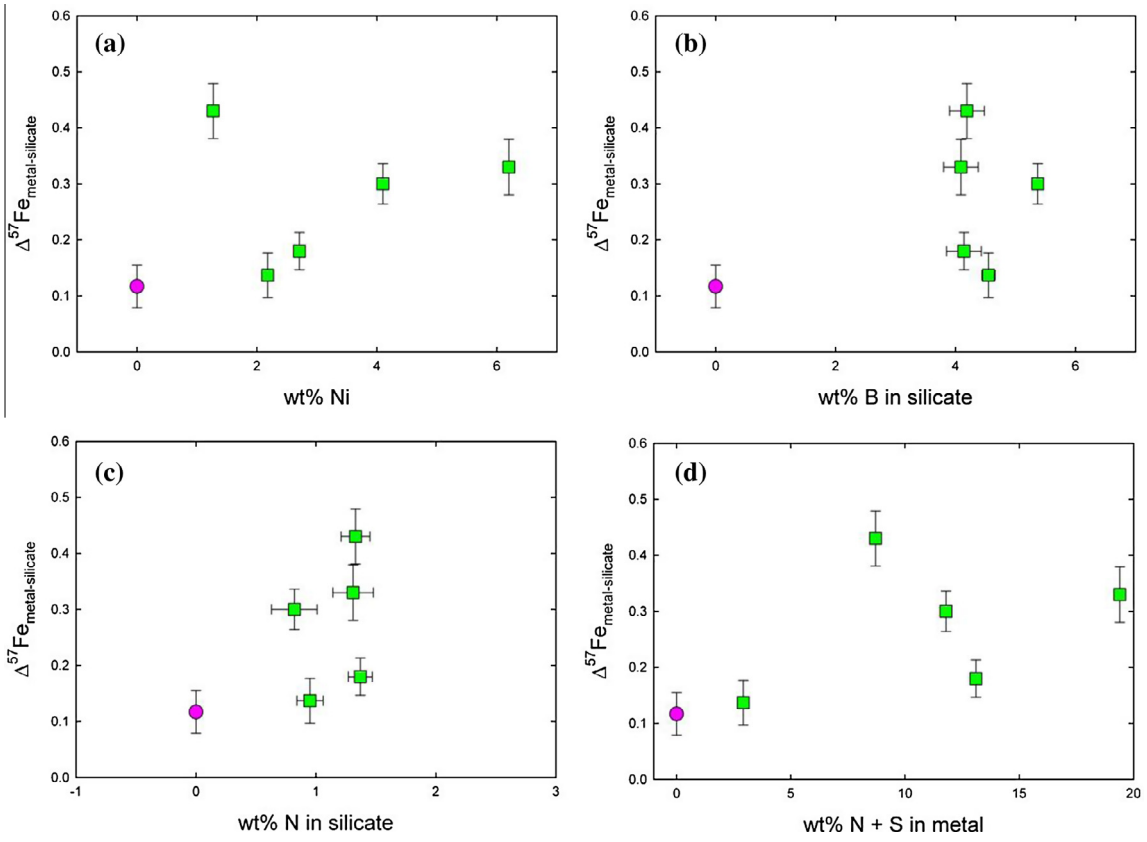

Fig. 5. $\Delta^{57}Fe_{metal-silicate}$ data plotted against (a) nickel content in the metal, (b) boron content in the silicate melt, (c) nitrogen content in the silicate melt and (d) nitrogen plus sulfur content in the metal. The green squares represent the Mars-like experiments whereas the pink circle represents the Earth-like experiment. The lack of correlation of $\Delta^{57}Fe_{metal-silicate}$ with all variables plotted is seen as further evidence that the fractionation measured in the experiments was controlled by sulfur concentration. (For interpretation of the references to colour in this figure legend, the reader is referred to the web version of this article.)

$$\delta^{56}Fe_i = \gamma\delta^{57}Fe_i + (\delta^{56}Fe_0 - \gamma\delta^{57}Fe_0) \quad (1)$$

which, relates the equilibrium Fe isotope ratios for phase i on the SFL where $\delta^{56}Fe_0$ and $\delta^{57}Fe_0$ are the δ values for the total Fe comprising the spiked experimental system. The last term is the intercept on the Fe three-isotope plot (Fig. 6).

In an earlier study, Shahar et al. (2008) found that, during an experiment, chemical equilibrium is achieved long before isotopic equilibrium (e.g., 6 h versus 48 h at 800 °C). From the present study, Fig. 6 shows the utility of the three-isotope technique for evaluating equilibrium from a pair of experiments that employed MgO capsules and Earth-like starting compositions. The SFL was calculated using the amount of spike added to the starting composition. In both experiments, the starting materials completely melted. The isotopic compositions of the metal fractions are identical to the bulk compositions because nearly all of the iron in the systems is in the metal. Both the metal compositions lie on the SFL. For a 5-min experimental runtime, the silicate glass composition lies off the SFL, demonstrating that isotopic equilibrium was not achieved in the run products. By contrast, for a separate experiment having a 120-min runtime, the Fe isotopic composition of the glass lies on the SFL. For the experiments in

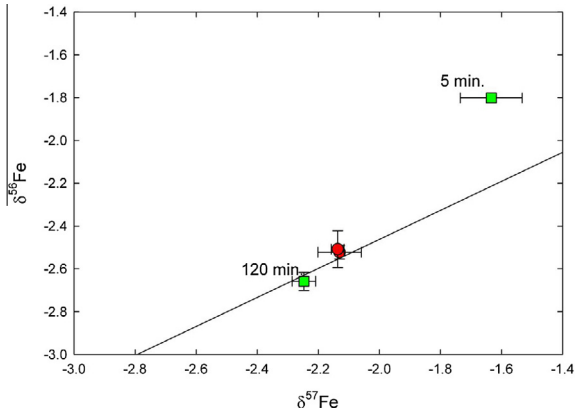

Fig. 6. Iron three-isotope plot compares the results of two experiments run for 2 different durations. Fe isotope compositions metal (in red) are identical for the two experiments and match the bulk compositions, because nearly all the Fe is contained in the metal. The green squares show the isotope compositions of the silicate glass. After 5 min run time, the silicate was not in isotopic equilibrium with the metal, as it lies off the calculated SFL. After 120 min runtime, however, the isotope compositions of the silicate lies on the SFL demonstrating that the system reached isotopic equilibrium. (For interpretation of the references to color in this figure legend, the reader is referred to the web version of this article.)

this study, isotopic equilibrium was reliably reached at 1650 °C after 120 min.

All experiments reported in this study reached isotopic equilibrium; that is, the isotope compositions of the metal and glass for each experiment lie on their respective calculated SFL. The reported $\Delta^{57}Fe_{metal-silicate}$ values were directly measured, not extrapolated from incompletely equilibrated run products to the SFL, as can be done for studies using the three isotope method (e.g., Shahar et al., 2008; Williams et al., 2012). The errors reported for $\Delta^{57}Fe_{metal-silicate}$ therefore do not need to include error magnification resulting from such extrapolation. Consideration of only fully equilibrated experiments prevents the risk of larger error envelopes that could result from overspiked experiments. Nevertheless, all experiments in this study were spiked at a similar level of approximately 0.1% of the FeO in the silicate starting material.

Accurate measurements of isotope fractionation between metal and glass also require that the glass be devoid of metal. For experiments that reach equilibrium, the isotope compositions of contaminated glass also would lie on the SFL, between the metal and pure glass compositions. All of our results show well-resolved fractionation between metal and silicate, suggesting that metal contamination in silicate is negligible, if at all present as discussed above.

4. DISCUSSION

4.1. Comparison with previous experimental studies

Our experimental results show a well-resolved Fe isotope fractionation between Fe alloy and silicate glass of $+0.12 \pm 0.04‰$ in a sulfur-free system. Isotope fractionation increases with sulfur content to $+0.43 \pm 0.03‰$ at 18% sulfur in the metal. Our experimental protocols were designed to try to overcome some of the complexities present in the interpretation of previous experimental studies of Fe isotope fractionation between Fe alloy and silicate. It is important to compare our results with previous results in the Fe metal–silicate system so as to explain the discrepancies in the literature. However, it is crucial to understand that experiments are very sensitive to temperature and composition and should therefore not be compared with each other unless they are in identical systems. As far as we are aware we have not duplicated any experiments already in the literature.

Isotopic equilibrium was obtained in all of our experiments, verified using the three isotope method. Isotopically equilibrated experiments also provide improved precision on the measurement of $\Delta^{57}Fe_{metal-silicate}$ because this value is directly calculated by subtraction of the isotopic compositions of the metal and silicate. Our uncertainties on these fractionations are <0.05‰. To calculate $\Delta^{57}Fe_{metal-silicate}$, Williams et al. (2012) used the intersections of the SFL with linear arrays of the Fe isotopic compositions from partially equilibrated experiments. The uncertainty on this intersection is far larger than the actual fractionations that we measured in our experiments and could be the reason for their larger fractionation between sulfur-free metal and silicate compared to this study, along with the pressure difference of the experiments. Further, we find that while most of the results of Poitrasson et al. (2009) are inconsistent with ours, for reasons that are not yet clear, there is one experiment that shows a slight resolvable $\Delta^{57}Fe_{metal-silicate} = +0.13 \pm 0.10‰$. This fractionation is in the same direction and within uncertainty of our fractionation of +0.17‰.

Our experiments used realistic compositions for a planetary core (i.e., an Fe–Ni alloy plus 0–17.5% S), as well as high enough temperatures so that the starting materials were completely melted. To investigate Fe isotope fractionation at lower temperatures at which fractionation should be enhanced, the study of Hin et al. (2012) added 25 wt.% Sn to their iron starting materials. No measurable Fe fractionation could be resolved between the resulting Fe–Sn alloy and silicate. It is unclear, however, how this amount of Sn would affect the bonding behavior of Fe during its segregation between alloy and silicate, and whether these results are directly comparable to ours. By adding a large amount of tin the bonding environment of iron in the melt would by definition be different than pure iron melt. One experiment from the same study added ~30 wt.% S, instead of Sn, to the starting composition. We suggest that such a large amount of S in the Fe metal starting materials, however, is probably more analogous to iron sulfide, not an Fe–S alloy as it is almost nearly at stoichiometric proportions (~36%). Results from both the Hin et al. experiments and our experiments can therefore be correct, as they are probing different systems. Previous studies of Fe fractionation between silicate and Fe-sulfide minerals (Williams et al., 2006; Schuessler et al., 2007; Polyakov and Soultanov, 2011) have inferred that, compared to their coexisting silicates, Fe sulfides are depleted in heavier Fe (other than pyrite). Such fractionation is in the opposite direction as that measured in our study in alloys. From this, we infer that Fe in alloys has different bonding structures than Fe in sulfide minerals.

The ratio of Fe^{2+} to Fe^{3+} in a system would affect Fe mass fractionation as well (Shahar et al., 2008; Dauphas et al., 2014). Therefore, it is interesting to evaluate if differences in oxygen fugacity can explain the different experimental results. With all the caveats mentioned in Section 3, we have calculated the oxygen fugacity conditions in our experiments to be between IW-1 and -2. Experiments by Poitrasson et al. (2009) were conducted at ~IW-2; experiments by Hin et al. (2012) were conducted between IW-0.5 and -2. If the difference between our sulfur-free results and the results of previous experiments were attributed only to different oxygen fugacities, then that would require that more than ~2/3 of the Fe in our experiments was in the 3^+ state (Shahar et al., 2008) which is not plausible at such reducing conditions. Because of the similarity of the fO_2 among all of these studies, we suspect that the differing iron isotope results instead are due to differences in starting compositions and experimental setup.

4.2. Controls on Fe isotope fractionation

Calculations of fractionation using vibrational frequencies of ^{57}Fe suggest that, at low pressures, silicate should have lighter Fe isotope compositions than metal

(Polyakov, 2009), consistent with our results. Why sulfur should increase iron isotope fractionation between metal and silicate is not immediately obvious and has not been theoretically calculated at the conditions of the current experiments. First-principles electronic structure of a liquid Fe–S alloy with 12 wt.% S at much higher pressures >300 GPa has been calculated (Alfè and Gillan, 1998). These calculations show that the covalent Fe–S bond is stronger than the metallic Fe–Fe bond, that sulfur atoms repel, and that the coordination number for the Fe–S bond is lower than for the Fe–Fe bond. These results suggest that the addition of S to an Fe alloy forms Fe–S bonds with a more covalent character. Because covalent bonds are stiffer (Schauble, 2004), they should be more enriched in ^{57}Fe and consequently enrich the alloy in ^{57}Fe. Increasing sulfur content in the alloy, therefore, should result in larger and more positive $\Delta^{57}Fe_{metal-silicate}$. If Fe–S bonding is more covalent also at the lower pressures examined in this study, then it could help explain the dependence of Fe fractionation with S content observed in our experiments.

4.3. Iron isotope fractionation during differentiation

The results of this study predict that Fe in a planetary body should be isotopically fractionated during differentiation of core and mantle. If the core materials comprise nearly 90% of the total Fe in a planetary body (McDonough, 2014), then they should reflect the isotopic composition of the planetary building blocks. If differentiation occurred at conditions and compositions similar to those of our experiments, then the silicate mantle should have Fe that is isotopically lighter by at least 0.1‰. Sulfur-bearing bodies would be expected to show larger Fe fractionations during differentiation, with the magnitude of the fractionation proportional to the sulfur content.

The iron isotope compositions of natural samples are difficult to understand from our current understanding of the mechanisms that affect them. Carbonaceous and ordinary chondrites yield uniform δ^{56}Fe values of -0.010 ± 0.010‰ and -0.013 ± 0.010‰, respectively, while enstatite chondrites yield a somewhat larger range from -0.14 ± 0.03‰ to $+0.12 \pm 0.03$‰ (Craddock and Dauphas, 2010). Iron in terrestrial abyssal peridotites is not resolvable from chondritic values (Craddock et al., 2013), while peridotite xenoliths and oceanic basalts average +0.1‰ (Poitrasson et al., 2013; Teng et al., 2013 and references therein). These results are interpreted to suggest that terrestrial mantle has Fe that is either indistinguishable from chondritic or heavier by +0.1‰. Further, Shergotty–Nahkla–Chasigny (SNC) meteorites from Mars and eucrite–diogenite (HED) meteorites thought to originate on the asteroid Vesta, also have chondritic iron isotope values (Poitrasson et al., 2004; Wang et al., 2012). Olivine and metal in pallasites (Poitrasson et al., 2005), by contrast, show Fe fractionation between those minerals in the same direction as predicted by the results in this study.

With the exception of one pallasite study (Poitrasson et al., 2005), no groups of natural samples, all of which in some way sample silicate mantles, have the light Fe isotope composition predicted by the results of this study for planetary bodies formed from chondritic building blocks. Possible explanations of this discrepancy are (1) these bodies did not form from materials having chondritic Fe or (2) additional parameters controlled Fe isotope fractionation during core–mantle. The pressure and temperature at which core–mantle differentiation occurs is largely uncertain, but probably has strong effects on the Fe isotope fractionation (Polyakov, 2009). For example, because isotope fractionation decreases in proportion to $1/T^2$ (Bigeleisen and Mayer, 1947), the fractionation may not be resolvable if Fe in the terrestrial core segregated at 3000–4000 °C, much higher than the temperature evaluated in this study. Further, calculations of fractionation using vibrational frequencies of ^{57}Fe suggest silicate should have lighter Fe isotope compositions than metal at low pressures (consistent with our results), but the direction of the fractionation changes at the ultra-high pressures near the core–mantle boundary (Polyakov, 2009). The oxidation state of Fe in the non-metal phase and particularly the presence of light elements (e.g., Si, C, O and H) in addition to sulfur in the metal may strongly affect iron isotope fractionation.

4.4. Differentiation on Mars, as an example

This study may shed light, in particular, on the formation and composition of Mars where sulfur has long been thought to be the main light element (e.g., Bertka and Fei, 1997). Isotope constraints from Martian meteorites suggest Mars accreted to more than half its final size within several Ma after Solar System formation, with sufficient heat-producing elements to produce silicate melting (Dauphas and Pourmand, 2011). Late accretion continued after core differentiation, but was completed before solidification of the final magma ocean within 60 Ma (Brandon et al., 2012). Martian meteorites have large heterogeneities in short-lived radionuclides ^{182}W and ^{142}Nd, and likely sample mantle reservoirs that formed by early crystallization of the final magma ocean (Foley et al., 2005). However, the iron isotopic ratios of all Martian meteorites are identical (Poitrasson et al., 2004; Weyer et al., 2005; Wang et al., 2012) demonstrating that iron isotopic compositions were not fractionated after solidification of the magma ocean. Any Fe isotopic fractionation produced by core formation, therefore, should still be measurable in the meteorites.

Fig. 7 shows the δ^{57}Fe of a Martian mantle predicted by our experimental results as a function of the weight% S in the core at several temperatures. The range of temperatures (2100 ± 100 K) of Martian differentiation is inferred from the contents of siderophile elements in Martian meteorites and experimentally determined distribution coefficients at 17% sulfur in the Martian core (Righter and Chabot, 2011). (Previous work (Chabot et al., 2005) has shown that the effect of S on Ni and Co partitioning is fairly minor.) If sulfur in the core were the only parameter controlling the δ^{57}Fe of the mantle and the SNC meteorites then, the results of this study predict that the meteorites should show a negative δ^{57}Fe. However, the SNC meteorites are chondritic (~0‰) and do not show this depletion.

Additional factors that might cause the slight discrepancy between the measured Fe isotope composition of

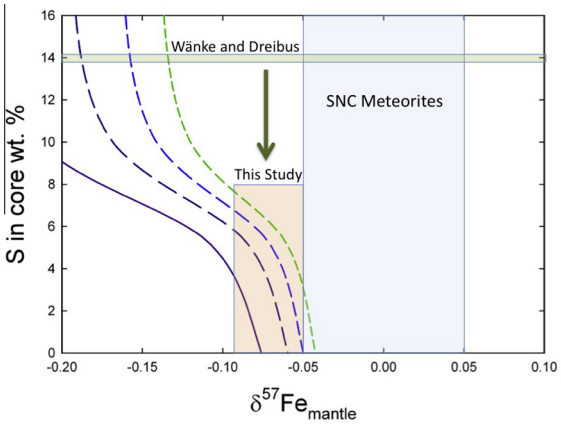

Fig. 7. The Fe isotope compositions expected for the Martian mantle for a range of S contents, based on the results of this study. The light blue box shows the range of δ^{57}Fe measured in Martian meteorites from the literature (Poitrasson et al., 2004; Weyer et al., 2005; Wang et al., 2012) along with an average of the 2SE reported in those studies. The curves show the δ^{57}Fe expected for Martian mantle that differentiated at different sulfur contents and temperatures. The solid curve shows the temperature (1923 K) at which the experiments in this study were conducted. The dotted curves represent the range of temperatures (2100 ± 100 K) of Martian differentiation inferred from the contents of siderophile elements in Martian meteorites and experimentally determined distribution coefficients (Righter and Chabot, 2011). The green box shows the Wanke and Dreibus, 1988 estimate for the sulfur content of the Martian core and the orange box shows the values from this study that are within error the SNC meteorite data when all errors in the measurements and within the model are taken into account. It can be seen that up to ~8 wt.% S can fit the data from this study even if no process has affected the iron isotope ratios post-differentiation. (For interpretation of the references to color in this figure legend, the reader is referred to the web version of this article.)

Martian meteorites and that predicted by our experimental results are: a higher temperature of core formation than previously reported, late accretion of chondritic material that reset the Fe isotopic signature of Mars mantle after core formation, or lack of a magma ocean that homogenized the Fe isotope composition of the mantle. To decrease the Fe isotope fractionation sufficiently to reproduce the Fe isotope compositions of the SNC meteorites would require core formation at >3500 K. Such a high temperature is unlikely because it is even higher than estimates for formation of Earth's core, which is much larger and has more heat producing elements. To erase the Fe isotope signature in the Martian mantle predicted by the formation of a S-rich core would require the accretion of more than 20% of material having chondritic Fe after core formation. This amount of late accretion is far more than the <1% estimated from highly siderophile element abundances in the Martian mantle (Bottke et al., 2010). Neither of these options, therefore, are particularly plausible explanations for the chondritic Fe isotope composition of SNC meteorites. These meteorites, nevertheless, curiously lack the Fe isotope signature that our work predicts for Martian mantle remaining after segregation of a high-sulfur Martian core.

A more plausible option is that there is less sulfur in the Martian core than some previous suggestions. Estimates for as much as 14% S in the Martian core are based on FeO contents for the Martian mantle derived from SNC meteorite compositions, assuming CI chondritic ratios for Fe (total), Si and Mg for Mars' bulk composition with all S partitioned into the core (Wänke and Dreibus, 1988). Although this value has been debated extensively, most authors favor >10 wt.% sulfur (e.g., Fei and Bertka, 2005). In contrast, experimental partitioning studies of transition metals support S concentrations in the Martian core of <1 wt.% (Gaetani and Grove, 1997). The concentration of sulfur in the Martian core is of utmost importance for understanding Mars' thermal evolution, its internal structure, and the generation and cessation of the early magnetic field. We can estimate a range of S contents for the Martian core, based on the Fe isotope fractionation factors determined in this study and assuming that nothing else has affected the Fe isotope composition of the Martian mantle during its long history. Taking into account all the errors associated with the measurements and experiments, we suggest the SNC Fe isotope compositions are consistent with a mantle source that had previously differentiated to form a core having ~6–9 wt.% S, However, to better constrain the extent of Fe isotope fractionation during differentiation processes, more experiments are needed in the iron alloy–silicate system.

With the exception of one pallasite study (Poitrasson et al., 2005), no groups of natural samples, all of which in some way sample silicate mantles, have the light Fe isotope composition predicted by the results of this study for planetary bodies formed from chondritic building blocks. Possible explanations of this discrepancy are (1) these bodies did not form from materials having chondritic Fe or (2) additional parameters controlled Fe isotope fractionation during core–mantle differentiation. The pressure and temperature at which core–mantle differentiation occurs is largely uncertain, but probably have strong effects on the Fe isotope fractionation (Polyakov, 2009). For example, because isotope fractionation decreases in proportion to $1/T^2$ (Bigeleisen and Mayer, 1947), the fractionation may not be resolvable if Fe in the terrestrial core segregated at 3000–4000 °C, much higher than the temperature evaluated in this study. Further, calculations of fractionation using vibrational frequencies of ^{57}Fe suggest silicate should have lighter Fe isotope compositions than metal at low pressures (consistent with our results), but the direction of the fractionation changes at the ultra-high pressures near the core-mantle boundary (Polyakov, 2009). The oxidation state of Fe in the non-metal phase and particularly the presence of light elements (e.g., Si, C, O and H) in addition to sulfur in the metal may strongly affect iron isotope fractionation.

5. CONCLUSIONS

Carefully designed experiments demonstrated resolvable Fe isotope fractionation between silicate and metal at 1–2 GPa, with the silicate enriched in lighter Fe. The extent of fractionation increases in proportion to the amount of

sulfur in the system. In a differentiated planetary body, the Fe isotope composition of the core should reflect the parental material because of mass balance constraints. The Fe isotope composition of the silicate mantle, by contrast, may place powerful constraints on the temperature and pressure of differentiation, and on the content of the light elements in the core. Iron in terrestrial rocks and meteorites that sample planetary mantles reflects these complex processes. More experimental work will help to better quantify the isotopic effects of the planetary compositions and conditions during core-mantle differentiation. Based on our experimental data, we suggest a decrease in the estimates of the concentration of sulfur in the Martian core with a maximum at ~8 wt.%.

ACKNOWLEDGMENTS

We are indebted to our geochemistry colleagues at GL and DTM for wonderful discussions that greatly enhanced the quality of this work. E. Hauri and J. Armstrong are thanked for help with ion probe and electron probe, respectively. L. Deng is thanked for help with experiments. F. Poitrasson, K. Wang, V. Polyakov and an anonymous reviewer are thanked for thoughtful reviews that helped make the manuscript stronger. M. Humayun is thanked for excellent editorial handling. Y. Fei is thanked for support and access to his lab. V.J.H. and the experimental facility are partially supported by NASA NNX11AC68G to Y. Fei. This work was funded by NSF Grants EAR0948131 and EAR1321858 to A.S.

REFERENCES

Alfè D. and Gillan M. J. (1998) First-principles simulations of liquid Fe–S under Earth's core conditions. *Phys. Rev. B* **58**, 8248.

Bertka C. M. and Fei Y. (1997) Mineralogy of the Martian interior up to core–mantle boundary pressures. *J. Geophys. Res.* **102**, 5251–5264.

Bigeleisen J. and Mayer M. G. (1947) Equilibrium constants for isotopic exchange reactions. *J. Chem. Phys.* **15**, 261–267.

Borg L. E., Connelly J. N., Boyet M. and Carlson R. W. (2011) Chronological evidence that the Moon is either young or did not have a global magma ocean. *Nature* **477**, 70–72.

Bottke W. F., Walker R. J., Day J. M. D., Nesvorny D. and Elkins-Tanton L. (2010) Stochastic late accretion to Earth, the Moon, and Mars. *Science* **330**, 1527–1530.

Brandon A. et al. (2012) Evolution of the Martian mantle inferred from the ^{187}Re–^{187}Os isotope and highly siderophile element abundance systematics of shergottite meteorites. *Geochim. Cosmochim. Acta* **76**, 206–235.

Caro G., Bourdon B., Birck J. and Moorbath S. (2006) High-precision ^{142}Nd/^{144}Nd measurements in terrestrial rocks: constraints on the early differentiation of the Earth's mantle. *Geochim. Cosmochim. Acta* **70**, 164–191.

Chabot N. L. (2004) Sulfur contents of the parental metallic cores of magmatic iron meteorites. *Geochim. Cosmochim. Acta* **68**, 3607–3618.

Chabot N. L. and Jones J. H. (2003) The parameterization of solid metal–liquid metal partitioning of siderophile elements. *Meteorit. Planet. Sci.* **38**, 1425–1436.

Chabot N. L., Draper D. S. and Agee C. (2005) Conditions of core formation in the earth: Constraints from nickel and cobalt partitioning. *Geochim. Cosmochim. Acta* **69**, 2141–2151.

Chabot N. L., McDonough W. F., Jones J. H., Saslow S. A., Ash R. D., Draper D. S. and Agee C. B. (2011) Partitioning behavior at 9 GPa in the Fe–S system and implications for planetary evolution. *Earth Planet. Sci. Lett.* **305**, 425–434.

Craddock P. R. and Dauphas N. (2010) Iron isotopic compositions of geological reference materials and chondrites. *Geostand. Geoanal. Res.* **35**, 101–123.

Craddock P. R., Warren J. M. and Dauphas N. (2013) Abyssal peridotites reveal the near-chondritic Fe isotopic composition of the Earth. *Earth Planet. Sci. Lett.* **365**, 63–76.

Dauphas N. and Pourmand A. (2011) Hf–W–Th evidence for rapid growth of Mars and its status as a planetary embryo. *Nature* **473**, 489–492.

Dauphas N. et al. (2009) Iron isotopes may reveal the redox conditions of mantle melting from Archean to present. *Earth Planet. Sci. Lett.* **288**, 255–267.

Dauphas N. et al. (2014) Magma redox and structural controls on iron isotope variations in Earth's mantle and crust. *Earth Planet. Sci. Lett.* **398**, 127–140.

Elkins-Tanton L. T. (2012) Magma Oceans in the inner solar system. *Annu. Rev. Earth Planet. Sci.* **40**, 113–139.

Fei Y. and Bertka C. (2005) The interior of Mars. *Science* **308**, 1120–1121.

Foley C. N., Wadhwa M., Borg L. E., Janney P. E. and Hines R. (2005) The early differentiation history of Mars from ^{182}W–^{142}Nd isotope systematics in the SNC meteorites. *Geochim. Cosmochim. Acta* **69**, 4557–4571.

Gaetani G. A. and Grove T. L. (1997) Partitioning of moderately siderophile elements among olivine, silicate melt, and sulfide melt: constraints on core formation in the Earth and Mars. *Geochim. Cosmochim. Acta* **61**, 1829–1846.

Hin R. C., Schmidt M. W. and Bourdon B. (2012) Experimental evidence for the absence of iron isotope fractionation between metal and silicate liquids at 1 GPa and 1250–1300 °C and its cosmochemical consequences. *Geochim. Cosmochim. Acta* **93**, 164–181.

Kleine T., Palme H. and Mezger R. K. (2005) Hf–W chronometry of lunar metals and the age and early differentiation of the Moon. *Science* **310**, 1671–1674.

Leroux P., Shirey S., Hauri E., Perfit M. and Bender J. (2006) The effects of variable sources, processes and contaminants on the composition of northern EPR MORB (8–10°N and 12–14°N): evidence from volatiles (H_2O, CO_2, S) and halogens (F, Cl). *Earth Planet. Sci. Lett.* **251**, 209–231.

Lodders K. (2000) An oxygen isotope mixing model for the accretion and composition of rocky planets. *Space Sci. Rev.* **92**, 341–354.

Matsuhisa J., Goldsmith J. R. and Clayton R. N. (1978) Mechanisms of hydrothermal crystallisation of quartz at 250 °C and 15 kbar. *Geochim. Cosmochim. Acta* **42**, 173–182.

McDonough W. F. (2014) Compositional model for the Earth's core. In *Treatise on Geochemistry* (eds. H. Holland and K. Turekian), second ed., vol. **3**. pp.559–577.

Moskovitz N. and Gaidos E. (2011) Differentiation of planetesimals and the thermal consequences of melt migration in the early solar system. *Meteorit. Planet. Sci.* **46**, 903–918.

Poitrasson F., Halliday A. N., Lee D.-C., Levasseur S. and Teutsch N. (2004) Iron isotope differences between Earth, Moon, Mars and Vesta as possible records of contrasted accretion mechanisms. *Earth Planet. Sci. Lett.* **223**, 253–266.

Poitrasson F., Levasseur S. and Teutsch N. (2005) Significance of iron isotope mineral fractionation in pallasites and iron meteorites for the core–mantle differentiation of terrestrial planets. *Earth Planet. Sci. Lett.* **234**, 151–164.

Poitrasson F., Roskosz M. and Corgne A. (2009) No iron isotope fractionation between molten alloys and silicate melt to 2000 °C and 7.7 GPa: experimental evidence and implications for

planetary differentiation and accretion. *Earth Planet. Sci. Lett.* **278**, 376–385.

Poitrasson F., Delpech G. and Gregoire M. (2013) On the iron isotope heterogeneity of lithospheric mantle xenoliths: implications for mantle metasomatism, the origin of basalts and the iron isotope composition of the Earth. *Contrib. Mineral. Petrol.* **165**, 1243–1258.

Polyakov V. B. (2009) Equilibrium iron isotope fractionation at core–mantle boundary conditions. *Science* **323**, 912–914.

Polyakov V. B. and Soultanov D. M. (2011) New data on equilibrium iron isotope fractionation among sulfides: constraints on mechanisms of sulfide formation in hydrothermal and igneous systems. *Geochim. Cosmochim. Acta* **75**, 1957–1974.

Ricolleau A., Fei Y., Corgne A., Siebert J. and Badro J. (2011) Oxygen and silicon contents of Earth's core from high pressure metal–silicate partitioning experiments. *Earth Planet. Sci. Lett.* **310**, 1–13.

Righter K. and Chabot N. L. (2011) Moderately and slightly siderophile element constraints on the depth and extent of melting in early Mars. *Meteorit. Planet. Sci.* **46**, 157–176.

Rushmer T., Petford N., Humayun M. and Campbell A. (2005) Fe-liquid segregation in deforming planetesimals: coupling Core–Forming compositions with transport phenomena. *Earth Planet. Sci. Lett.* **239**, 185–202.

Sanloup C. and Fei Y. (2004) Closure of the Fe–S–Si liquid miscibility gap at high pressure. *Phys. Earth Planet. Inter.* **147**, 57–65.

Schauble E. A. (2004) Applying stable isotope fractionation theory to new systems. *Rev. Mineral. Geochem.* **55**, 65–111.

Schuessler J. A., Schoenberg R., Behrens H. and von Blanckenburg F. (2007) The experimental calibration of the iron isotope fractionation factor between pyrrhotite and peralkaline rhyolitic melt. *Geochim. Cosmochim. Acta* **71**, 417–433.

Shahar A., Young E. D. and Manning C. E. (2008) Equilibrium high-temperature Fe isotope fractionation between fayalite and magnetite: an experimental calibration. *Earth Planet. Sci. Lett.* **268**, 330–338.

Strelow F. (1980) Improved separation of iron from copper and other elements by anion-exchange chromatography on a 4% cross-linked resin with high concentrations of hydrochloric acid. *Talanta* **27**, 727–732.

Taylor G. (1992) Core formation in asteroids. *J. Geophys. Res.* **97**, 14717–14726.

Teng F.-Z., Dauphas N., Huang S. and Marty B. (2013) Iron isotopic systematics of oceanic basalts. *Geochim. Cosmochim. Acta* **107**, 12–26.

Wang K. et al. (2012) Iron isotope fractionation in planetary crusts. *Geochim. Cosmochim. Acta* **89**, 31–45.

Wänke H. and Dreibus G. (1988) Chemical composition and accretion history of terrestrial planets. *Philos. Trans. R. Soc. A* **325**, 545–557.

Weyer S. et al. (2005) Iron isotope fractionation during planetary differentiation. *Earth Planet. Sci. Lett.* **240**, 251–264.

Wheeler K. T., Walker D., Fei Y., Minarik W. G. and McDonough W. F. (2006) Experimental partitioning of uranium between liquid iron sulfide and liquid silicate: implications for radioactivity in the Earth's core. *Geochim. Cosmochim. Acta* **70**, 1537–1547.

Williams H. M. et al. (2006) Fe isotope fractionation in iron meteorites: new insights into metal-sulphide segregation and planetary accretion. *Earth Planet. Sci. Lett.* **250**, 486–500.

Williams H. M., Wood B. J., Wade J., Frost D. J. and Tuff J. (2012) Isotopic evidence for internal oxidation of the Earth's mantle during accretion. *Earth Planet. Sci. Lett.* **321–322**, 54–63.

Associate editor: Munir Humayun